PHYSICAL REVIEW D **80,** 126018 (2009)

Particle production during inflation: Observational constraints and signatures

Neil Barnaby* and Zhiqi Huang†

Canadian Institute for Theoretical Astrophysics, University of Toronto, McLennan Physical Laboratories, 60 St. George Street, Toronto, Ontario, Canada M5S 3H8

(Received 29 September 2009; published 29 December 2009)

In a variety of inflation models the motion of the inflaton may trigger the production of some noninflaton particles during inflation, for example, via parametric resonance or a phase transition. Particle production during inflation leads to observables in the cosmological fluctuations, such as features in the primordial power spectrum and also non-Gaussianities. Here we focus on a prototype scenario with inflaton, ϕ, and isoinflaton, χ, fields interacting during inflation via the coupling $g^2(\phi - \phi_0)^2\chi^2$. Since several previous investigations have hinted at the presence of localized "glitches" in the observed primordial power spectrum, which are inconsistent with the simplest power-law model, it is interesting to determine the extent to which such anomalies can be explained by this simple and microscopically well-motivated inflation model. Our prototype scenario predicts a bumplike feature in the primordial power spectrum, rather than an oscillatory "ringing" pattern as has previously been assumed. We discuss the observational constraints on such features using a variety of cosmological data sets. We find that bumps with amplitudes as large as $\mathcal{O}(10\%)$ of the usual scale-invariant fluctuations from inflation, corresponding to $g^2 \sim 0.01$, are allowed on scales relevant for cosmic microwave background experiments. Our results imply an upper limit on the coupling g^2 (for a given ϕ_0) which is crucial for assessing the detectability of the non-Gaussianity produced by inflationary particle production. We also discuss more complicated features that result from superposing multiple instances of particle production. Finally, we point to a number of microscopic realizations of this scenario in string theory and supersymmetry and discuss the implications of our constraints for the popular brane/axion monodromy inflation models.

DOI: 10.1103/PhysRevD.80.126018 PACS numbers: 11.25.Wx, 98.80.Cq

I. INTRODUCTION

Recently, there has been considerable interest in inflationary models where the motion of the inflaton triggers the production of some noninflation (isocurvature) particles *during* inflation [1–17]. Examples have been studied where this particle production occurs via parametric resonance [1–6], as a result of a phase transition [7–13], or otherwise. In some scenarios, backreaction effects from particle production can slow the motion of the inflaton on a steep potential [14–16], providing a new inflationary mechanism. Moreover, inflationary particle production arises naturally in a number of realistic microscopic models from string theory [14–16,18–20] and also from supersymmetry (SUSY) [21].

In [5] it was shown that the production of massive isocurvature particles during inflation (and their subsequent interactions with the slow-roll condensate) provides a qualitatively new mechanism for generating cosmological perturbations. This new mechanism leads to a variety of novel observable signatures, such as features [5] and non-Gaussianities [5,22] in the primordial fluctuations. In this paper we study in detail the observational constraints on such distortions of the primordial power spectrum for a variety of scenarios.

One motivation for this study is to determine whether features generated by particle production during inflation can explain some of the anomalies in the observed primordial power spectrum, $P(k)$. A number of different studies have hinted at the possible presence of some localized features in the power spectrum [2,13,23–34], which are not compatible with the simplest power-law $P(k) \sim k^{n_s-1}$ model. Although such glitches may simply be statistical anomalies, there is also the tantalizing possibility that they represent a signature of primordial physics beyond the simplest slow-roll inflation scenario. Forthcoming polarization data may play a crucial role in distinguishing between these possibilities [13]. However, in the meantime, it is interesting to determine the extent to which such features may be explained by microscopically realistic inflation models.

We consider a very simple model where the inflaton, ϕ, and isoinflaton, χ, fields interact via the coupling

$$\mathcal{L}_{\rm int} = -\frac{g^2}{2}(\phi - \phi_0)^2\chi^2. \tag{1}$$

We focus on this simple prototype model in order to illustrate the basic phenomenology of particle production during inflation; however, we expect our results to generalize in a straightforward way to more complicated scenarios. Models of the type (1) have been considered as a probe

*barnaby@cita.utoronto.ca,
†zqhuang@astro.utoronto.ca

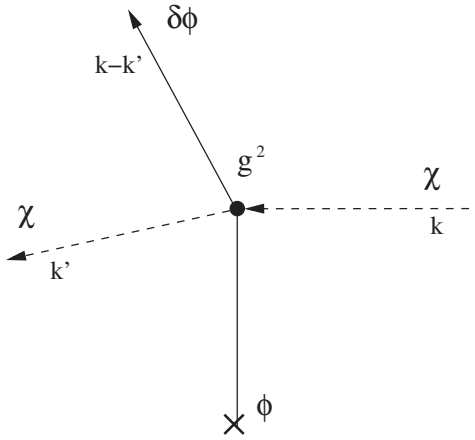

FIG. 1. Rescattering diagram.

of Planck-scale effects [1] and offer a novel example of the nondecoupling of high energy physics during inflation.[1]

At the moment when $\phi = \phi_0$ (which we assume occurs during the observable range of e-foldings of inflation), the χ particles become instantaneously massless and are produced by quantum effects. This burst of particle production drains energy from the condensate $\phi(t)$, temporarily slowing the motion of the inflaton background and violating slow roll. Shortly after this moment, the χ particles become extremely nonrelativistic, so that their number density dilutes as a^{-3}, and eventually the inflaton settles back onto the slow-roll attractor.

Several previous papers [1–4] have studied the temporary slowing down of the inflaton background using the mean-field equation

$$\ddot{\phi} + 3H\dot{\phi} + V_{,\phi} + g^2(\phi - \phi_0)\langle\chi^2\rangle = 0, \qquad (2)$$

where the vacuum average $\langle\chi^2\rangle$ is computed following [36,37]. Using this approach one finds that the transient violation of slow roll leads to a "ringing pattern" (damped oscillations) in the spectrum of cosmological fluctuations leaving the horizon near the moment when $\phi = \phi_0$ [4]. In [2,3] observational constraints on particle production during inflation were discussed in the context of this mean-field treatment.

However, in [5] cosmological fluctuations in the model (1) were reconsidered, going beyond the mean-field treatment of ϕ.[2] It was pointed out that the massive χ particles can rescatter off the condensate to generate bremsstrahlung radiation of long-wavelength $\delta\phi$ fluctuations via diagrams such as Fig. 1. Multiple rescattering processes lead to a rapid cascade of power into the IR—*IR cascading*. The inflaton modes generated by IR cascading freeze once their wavelengths cross the horizon, and lead to a bumplike feature in the cosmological perturbations that is illustrated in Fig. 2. This feature is complementary to the usual (nearly) scale-invariant quantum vacuum fluctuations from inflation. The bump dominates over the ringing pattern discussed above by many orders of magnitude, independently of the value of g^2.

In light of the results of [5] it is clear that the observational constraints on the model (1) need to be reconsidered. Since previous studies have suggested marginal evidence for localized power excesses in the CMB using both parametric [2,33] and nonparametric [30,31] techniques, it is interesting to determine if a simple and well-motivated model such as (1) can explain these anomalies. To answer this question we provide a simple semianalytic fitting function that accurately captures the shape of the feature generated by particle production and IR cascading during inflation. Next, we confront this modified power spectrum with a variety of observational data sets. We find no evidence for a detection; however, we note that observations are consistent with relatively large spectral distortions of the type predicted by model (1). If the feature is located on scales relevant for CMB experiments, then its

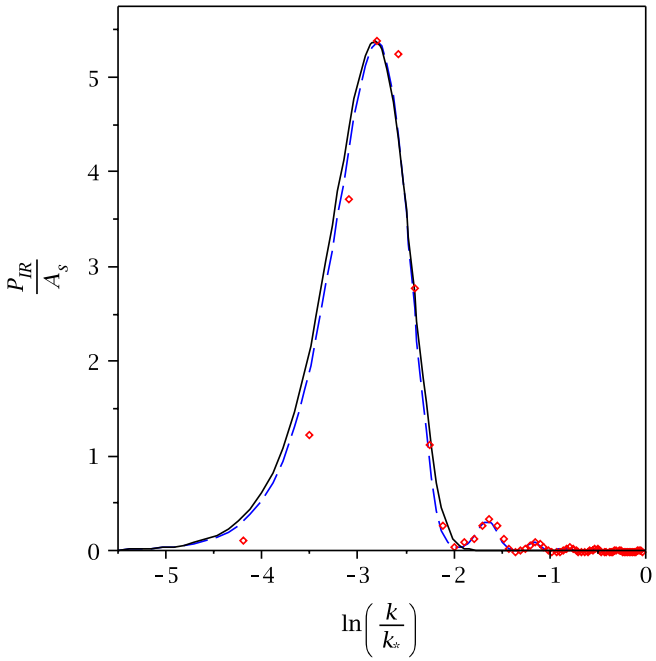

FIG. 2 (color online). The bumplike features generated by IR cascading. We plot the feature power spectrum obtained from fully nonlinear lattice field theory simulations (red points) and also the result of an analytical calculation (dashed blue curve) using the formalism described in [38]. We also superpose the fitting function $\sim k^3 e^{-\pi k^2/(2k_*^2)}$ (solid black curve) to illustrate the accuracy of this simple formula.

[1]For reasonable values of g^2 the χ particles are *extremely* massive for almost the entire duration of inflation except for a tiny interval, much less than an e-folding, about the point $\phi = \phi_0$. However, the χ field cannot be integrated out due to the nonadiabatic time dependence of the mode functions; see [35] for further discussion.

[2]See also [15] for a complimentary analysis and [38] for a detailed analytical treatment of the dynamics.

amplitude may be as large as $\mathcal{O}(10\%)$ of the usual scale-invariant fluctuations, corresponding to $g^2 \sim 0.01$. Our results translate into a ϕ_0-dependent bound on the coupling g^2, which is crucial in order to determine whether the non-Gaussian signal associated with particle production and IR cascading is detectable in future missions [22].

We also consider the more complicated features which result from multiple bursts of particle production and IR cascading. Such features are a prediction of a number of string theory inflation models, including brane/axion monodromy [18–20]. For an appropriate choice of the spacing between the features, we find that the constraint on g^2 in this scenario is even weaker than the single-bump case.

Although we focus on the interaction (1), our findings may also have some bearing on models with phase transitions during inflation. A simple prototype model for the latter scenario is

$$V(\phi, \chi) = \frac{\lambda}{4}(\chi^2 - v^2)^2 + \frac{g^2}{2}\chi^2\phi^2 + V_{\rm inf}(\phi).$$

At the moment when $\phi = \sqrt{\lambda}v/g$, massive isoinflaton χ particles are produced copiously by tachyonic (spinodal) instability [39]. These produced particles will subsequently interact with the condensate via rescattering diagrams similar to Fig. 1. Hence, we expect the features produced by inflationary phase transitions to be qualitatively similar to the bumps considered in this paper. (This intuition is consistent with a second-order computation of the cosmological perturbations in a closely related model [10]. See [33] for a discussion of the observational consequences.)

In the literature it is sometimes argued that inflationary phase transitions can be studied using a toy model with a sharp steplike feature in the inflaton potential. This potential-step model predicts a ringing pattern in the power spectrum, very much analogous to the mean-field treatment of resonant particle production during inflation, discussed above. This treatment does not take into account the violent growth of inhomogeneities of the fields that occurs during realistic phase transitions [39] and, in particular, does not capture rescattering effects and IR cascading. In the case of resonant particle production, these nonlinear effects have a *huge* impact on the cosmological fluctuations [5]. Hence, it is far from clear if the potential-step model provides a good effective description of inflationary phase transitions.[3]

Of course, inflation models with steps in $V(\phi)$ (or its derivatives) may be considered on phenomenological grounds, irrespective of the motivation from inflationary phase transitions. In [41,42] cosmological perturbations from models with steplike features and discontinuities in higher derivatives were considered, as were the microscopic motivations for such constructions. See [43,44] for a study of the non-Gaussianities induced in a variety of single-field models with steps or oscillations in the inflaton potential.

The outline of this paper is as follows. In Sec. II we provide a simple parametrization of the features that are imprinted on the primordial power spectrum by one or more bursts of particle production during inflation. In Sec. III we describe our method and discuss the observational data sets employed to derive constraints on this modified power spectrum. In Sec. IV we present observational constraints on various scenarios. In Sec. V we present some microscopic realizations of our scenario and discuss the implications of our findings for popular string theory/SUSY inflation models with a special emphasis on brane monodromy. Finally, in Sec. VI we conclude.

II. A SIMPLE PARAMETRIZATION OF THE POWER SPECTRUM

In [5] it was shown that particle production and IR cascading during inflation in the model (1) generate a bumplike contribution to the primordial power spectrum. As shown in Fig. 2, this feature can be fit with a very simple function $P_{\rm bump} \sim k^3 e^{-\pi k^2/(2k_\star^2)}$. The bumplike contribution from IR cascading is complementary to the usual (nearly) scale-invariant contribution to the primordial power spectrum $P_{\rm vac} \sim k^{n_s-1}$ coming from the quantum vacuum fluctuations of the inflaton. The total observable power spectrum in the model (1) is simply the superposition of these two contributions: $P(k) \sim k^{n_s-1} + k^3 e^{-\pi k^2/(2k_\star^2)}$. This simple formula can be motivated from analytical considerations [5,38] and provides a good fit to lattice field theory simulations near the peak of the feature and also in the IR tail.[4]

It is straightforward to generalize this discussion to allow for multiple bursts of particle production during inflation. Suppose there are multiple points $\phi = \phi_i$ $(i = 1, \cdots, n)$ along the inflationary trajectory where new degrees of freedom χ_i become massless:

$$\mathcal{L}_{\rm int} = -\sum_{i=0}^{n} \frac{g_i^2}{2}(\phi - \phi_i)\chi_i^2. \tag{3}$$

For each instant t_i when $\phi = \phi_i$, there will be an associated burst of particle production and subsequent rescattering of the produced massive χ_i off the condensate $\phi(t)$. Each of these events proceeds as described above and leads to a new bumplike contribution to the power spectrum. These features simply superpose owing to the fact that each field χ_i is statistically independent (so that the cross terms involving $\chi_i\chi_j$ with $i \neq j$ in the computation of the two-point function must vanish). Thus, we arrive at the follow-

[3] See also [40] for a related discussion.

[4] This fitting formula does *not* capture the small oscillatory structure in the UV tail of the feature (see Fig. 2), which does not concern us since that region is not phenomenologically interesting.

ing parametrization of the primordial power spectrum in models with particle production during inflation:

$$P(k) = A_s\left(\frac{k}{k_0}\right)^{n_s-1} + \sum_{i=1}^{n} A_i\left(\frac{\pi e}{3}\right)^{3/2}\left(\frac{k}{k_i}\right)^3 e^{-(\pi/2)(k/k_i)^2}, \quad (4)$$

where A_s is the amplitude of the usual nearly scale-invariant vacuum fluctuations from inflation and k_0 is the pivot, which we choose to be $k_0 = 0.002$ Mpc^{-1} following [45]. The constants A_i depend on the couplings g_i^2 and measure the size of the features from particle production. We have normalized these amplitudes so that the power in the ith bump, measured at the peak of the feature, is given by A_i. The location of each feature, k_i, is related to the number of e-foldings N from the end of inflation to the time when the ith burst of particle production occurs: roughly $\ln(k_i/H) \sim N_i$, where $N = N_i$ at the moment when $\phi = \phi_i$. From a purely phenomenological perspective the locations k_i are completely arbitrary.

We compare (4) to lattice field theory simulations in order to determine the amplitude A_i in terms of model parameters. We find

$$A_i \cong 1.01 \times 10^{-6} g_i^{15/4}. \quad (5)$$

Assuming standard chaotic inflation $V = m^2\phi^2/2$, we have tested this formula for $g^2 = 1, 0.1, 0.01$, taking both $\phi_0 = 2M_p$ and $\phi_0 = 3.2M_p$. We found agreement up to factors of order unity in all cases.

Theoretical consistency of our calculation of the shape of the feature bounds the couplings as $10^{-7} \lesssim g_i^2 \lesssim 1$ [5]. Hence, the power spectrum (4) can be obtained from sensible microphysics only when $10^{-20} \lesssim A_i \lesssim 10^{-6}$. This constraint still allows for a huge range of observational possibilities: Near the upper bound the feature is considerably larger than the vacuum fluctuations, while near the lower bound the feature is completely undetectable.

Note that for each bump in (4) the IR tail $P_{\rm bump} \to k^3$ as $k \to 0$ is similar to the feature considered by Hoi, Cline, and Holder in [33], consistent with causality arguments about the generation of curvature perturbations by local physics.

III. DATA SETS AND ANALYSIS

The primordial power spectrum for our model is parametrized as (4). Our aim is to derive observational constraints on the various model parameters A_s, n_s, k_i, and A_i using CMB, galaxy power spectrum, and weak lensing data. To this end we use the COSMOMC package [46] to run Markov Chain Monte Carlo (MCMC) calculations to determine the likelihood of the cosmological parameters, including our new parameters A_i and k_i. We employ the following data sets.

Cosmic microwave background:
Our complete CMB data sets include Wilkinson Microwave Anisotropy Probe (WMAP) 5 yr [45,47], BOOMERANG [48–50], Arcminute Cosmology Bolometer Array Receiver (ACBAR) [51–54], Cosmic Background Imager (CBI) [55–58], Very Small Array [59], DASI [60,61], and MAXIMA [62]. We have included the Sunyaev-Zel'dovich (SZ) secondary anisotropy [63,64] for WMAP 5 yr, ACBAR, and CBI data sets. The SZ template is obtained from hydrodynamical simulation [65]. Also included for theoretical calculation of CMB power spectra is the CMB lensing contribution.

Type Ia supernova (SN):
We employ the union supernova Ia data (307 SN Ia samples) from The Supernova Cosmology Project [66].

Large scale structure (LSS):
The 2dF Galaxy Redshift Survey (2dFGRS) data [67] and Sloan Digital Sky Survey (SDSS) Luminous Red Galaxy (LRG) data release 4 [68] are utilized.
Note that we have used the likelihood code based on the nonlinear modeling by Tegmark *et al.* [68] (marginalizing the bias b and the Q parameter). However, with a large bump in the linear power spectrum, this naive treatment may not be sufficient to characterize the nonlinear response to the feature on small scales. Ideally, this should be obtained from N-body simulations; however, such a study is beyond the scope of the current work.
There are several other caveats on our results in the high-k regime. First, we assume linear bias for the galaxies, which may not be entirely safe at sufficiently small scales. Moreover, sharp features in the matter power spectrum can cause sharp features in the bias as a function of k.
Keeping these caveats in mind, our constraints on small scales, $k \gtrsim 0.1$ Mpc^{-1}, should be taken with a grain of salt and considered as accurate only up to factors of order unity.

Weak lensing (WL):
Five WL data sets are used in this paper. The effective survey area $A_{\rm eff}$ and galaxy number density $n_{\rm eff}$ of each survey are listed in Table I.
For COSMOS data we use the COSMOMC plug-in written by Lesgourgues [70], modified to do numerical marginalization on three nuisance parameters in the original code.
For the other four weak lensing data sets, we use the likelihood given by [76]. To calculate the likelihood, we have written a COSMOMC plug-in code, with simplified marginalization on the parameters of galaxy number density function $n(z)$. More details about this plug-in can be found in [77].
As for the LSS data, for small scales $k \gtrsim 0.1$ Mpc^{-1} there is the caveat that the nonlinear evolution of the power

TABLE I. Weak lensing data sets.

Data sets	$A_{\rm eff}$ (deg^2)	$n_{\rm eff}$ (arcmin^{-2})
COSMOS [69,70]	1.6	40
CFHTLS-wide [71,72]	22	12
GaBODS [73,74]	13	12.5
RCS [73,74]	53	8
VIRMOS-DESCART [72,75]	8.5	15

spectrum in the presence of bumplike distortions may not be treated accurately.

IV. OBSERVATIONAL CONSTRAINTS

We now present our results for the observational constraints on particle production during inflation, assuming two different scenarios.

A. A single burst of particle production

The minimal scenario to consider is a single burst of particle production during inflation, which corresponds to taking $n = 1$ in (3). The power spectrum is given by (4) with $n = 1$ and, with some abuse of notation, we denote $k_1 \equiv k_{\rm IR}$ and $A_1 \equiv A_{\rm IR}$. The prior we have used for $A_{\rm IR}$ is $0 \leq A_{\rm IR} \leq 25 \times 10^{-10}$, and for $k_{\rm IR}$ it is $-9.5 \leq \ln[k/{\rm Mpc}^{-1}] \leq 1$. The former condition ensures that the bumplike feature from IR cascading does not dominate over the observed scale-invariant fluctuations, while the latter is necessary in order to have the feature in the observable range of scales. In Fig. 3 we plot the marginalized posterior likelihood for the new parameters $A_{\rm IR}$ and $k_{\rm IR}$ describing the magnitude and location of the bump, while in Table II we give the best-fit values for the remaining (vanilla) cosmological parameters.

For very large scales $\lesssim {\rm Gpc}^{-1}$, the data do not contain much information (due to cosmic variance) and hence the constraint on any modification of the power spectrum is weak. In this region the spectral distortion may be larger than 100% of the usual scale-invariant fluctuations and couplings g^2 order unity are allowed. For smaller scales, $k \gtrsim {\rm Gpc}^{-1}$, the constraints are stronger and we have, very roughly, $A_{\rm IR}/A_s \lesssim 0.1$ corresponding to $g^2 \lesssim 0.01$. For very small scales, $k \gtrsim 0.1\ {\rm Mpc}^{-1}$, our constraints should be taken with a grain of salt since the nonlinear evolution of the power spectrum may not be modeled correctly in the presence of bumplike distortions. At small scales nonlinear effects tend to wipe out features of this type (see, for example, [78]) and hence observational constraints for $k \gtrsim 0.1\ {\rm Mpc}^{-1}$ may be weaker than what is presented in Fig. 3. Note that in most of this nonlinear regime we find essentially no constraint on $A_{\rm IR}$, which is consistent with what would be expected in a more comprehensive treatment.

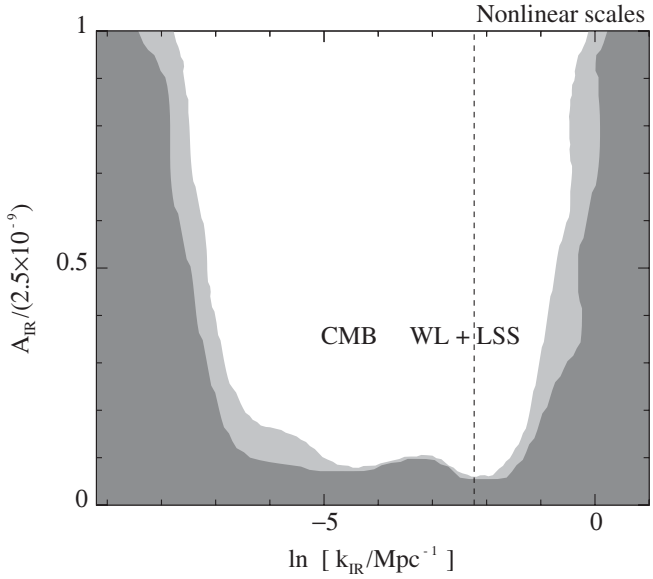

FIG. 3. Marginalized posterior likelihood contours for the parameters $A_{\rm IR}$ and $k_{\rm IR}$ (the magnitude and position of the feature, respectively) in the single-bump model. Black and grey regions correspond to parameter values allowed at 95.4% and 99.7% confidence levels, respectively. At small scales, to the right of the dashed vertical line, our results should be taken with a grain of salt since the nonlinear evolution of the power spectrum may not be modeled correctly in the presence of bumplike distortions.

TABLE II. Constraints on the standard ("vanilla") cosmological parameters for the single-bump model. All errors are at the 95.4% confidence level.

$\Omega_b h^2$	$0.0227^{+0.0010}_{-0.0010}$
$\Omega_c h^2$	$0.1122^{+0.0050}_{-0.0044}$
θ	$1.0424^{+0.0042}_{-0.0043}$
τ	$0.08^{+0.03}_{-0.03}$
n_s	$0.956^{+0.024}_{-0.024}$
$\ln[10^{10} A_s]$	$3.206^{+0.074}_{-0.068}$
$A_{\rm SZ}$	$1.62^{+0.76}_{-0.74}$
Ω_m	$0.264^{+0.026}_{-0.022}$
σ_8	$0.807^{+0.034}_{-0.030}$
z_{re}	$10.5^{+2.5}_{-2.7}$
H_0	$71.6^{+2.3}_{-2.4}$

The IR cascading bump in the primordial power spectrum will be accompanied by a corresponding non-Gaussian feature in the bispectrum [5,22]. From the perspective of potentially observing this signal, it is most interesting if this feature is located on scales probed by CMB experiments. (There is also the fascinating possibility that the non-Gaussianity from IR cascading could show up in the large scale structure as in [79–82]. We leave a detailed discussion to future studies.) To get some intuition into what kinds of features in the CMB scales are still allowed by the data, we focus on an example with $A_{\rm IR} = 2.5 \times 10^{-10}$ which, using (5), corresponds to a reasonable coupling value $g^2 \sim 0.01$. We take the bump to be located at $k_{\rm IR} = 0.01\ {\rm Mpc}^{-1}$ and fix the remaining model parameters to $A_s = 2.44 \times 10^{-9}$, $n_s = 0.97$ (which are compatible with the usual values). This sample bump in the power spectrum is illustrated in the top panel of Fig. 4 and is consistent with the data at 2σ. In the bottom panel of Fig. 4 we plot the associated angular CMB temperature-temperature (TT) spectrum. This example represents a surprisingly large spectral distortion: The total power in the feature as compared to the scale-invariant vacuum fluctuations is $P_{\rm bump}/P_{\rm vac} \sim 0.1$, evaluated at the peak of the bump. In [22] we discuss the non-Gaussianity associated with this feature.

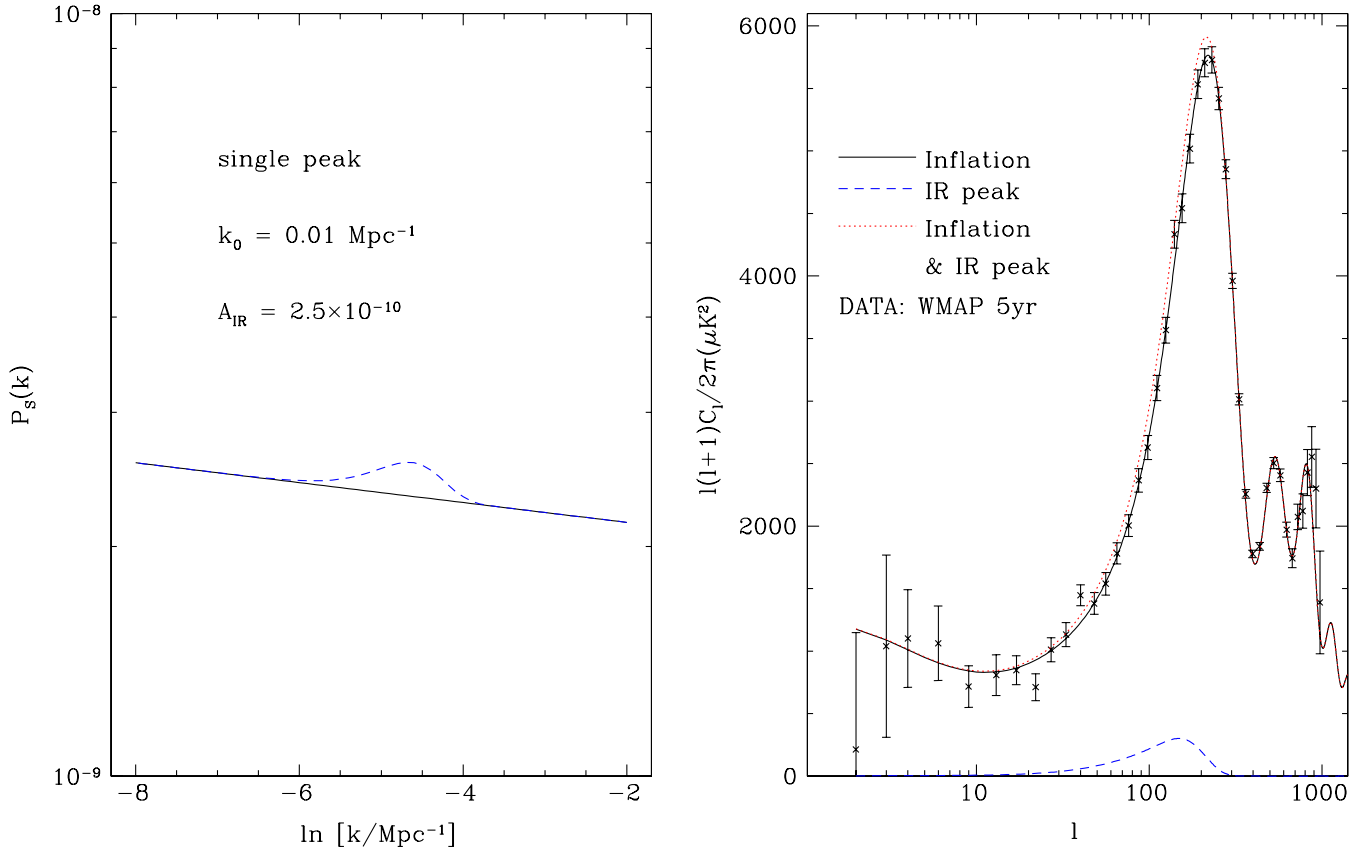

FIG. 4 (color online). The top panel shows a sample bump in the power spectrum with amplitude $A_{\rm IR} = 2.5 \times 10^{-10}$ which corresponds to a coupling $g^2 \sim 0.01$. The feature is located at $k_{\rm IR} = 0.01$ Mpc^{-1}. This example represents a distortion of $\mathcal{O}(10\%)$ as compared to the usual vacuum fluctuations and is consistent with the data at 2σ. The bottom panel shows the CMB angular TT power spectrum for this example, illustrating that the distortion shows up mostly in the first peak.

B. Multiple bursts of particle production

Next, we consider a slightly more complicated scenario: multiple bursts of particle production leading many localized features in the power spectrum. For simplicity, we assume that all bumps have the same magnitude $A_i \equiv A_{\rm IR}$ and we further suppose a fixed number of e-foldings δN between each burst of particle production. This implies that the location of the ith bump will be given by $k_i = e^{(i-1)\Delta} k_1$, where Δ is a model parameter controlling the density of features. We take the number of bursts, n, to be sufficiently large that the series of features extends over the whole observable range. In the next section we will see that these assumptions are not restrictive and that many well-motivated models are consistent with this simple setup.

Our multibump model, then, has three parameters: $A_{\rm IR}$, k_1, and Δ. We take the prior on the amplitude to be $A_{\rm IR} \leq 25 \times 10^{-10}$ as in Sec. IV A. If the features are very widely spaced, $\Delta \gtrsim 1$, then the constraint on each bump will obviously be identical to the results for the single-bump case presented in Sec. IV A. Hence the most interesting case to consider is $\Delta \lesssim 1$ so that the bumps are partially overlapping. Our prior for the density of features is therefore $0 \leq \Delta \leq 1$. Finally, the location of the first bump will be a historical accident in realistic models; hence we marginalize over all possible values of k_1 and present our constraints and 2d likelihood plots in the space of $A_{\rm IR}$ and Δ. This marginalized likelihood plot is presented in Fig. 5. In Table III we present the best-fit values for the vanilla cosmological parameters.

From the likelihood plot, Fig. 5, there is evidently a preferred value of the feature spacing, roughly $\Delta \sim 0.75$, for which the constraints are weakest. This can be understood as follows. For very high density $\Delta \to 0$ the localized features from IR cascading smear together and the total power spectrum (4) is $P(k) \sim A_s (k/k_0)^{n_s - 1} + C$, where the size of the constant deformation scales linearly with the density of features: $C \propto \Delta^{-1}$. Therefore, the upper bound on the amplitude $A_{\rm IR}$ should scale linearly with Δ. Indeed, this linear trend is very evident from Fig. 5 in the small-Δ regime. This linear behavior must break down at some point since as the features become infinitely widely spaced the constraint on $A_{\rm IR}$ must go to zero. This explains the bump in the likelihood plot, Fig. 5, near $\Delta \sim 0.75$.

In passing, notice that the behavior $P(k) \sim A_s (k/k_0)^{n_s - 1} + C$ for $\Delta \ll 1$ also explains why the best-

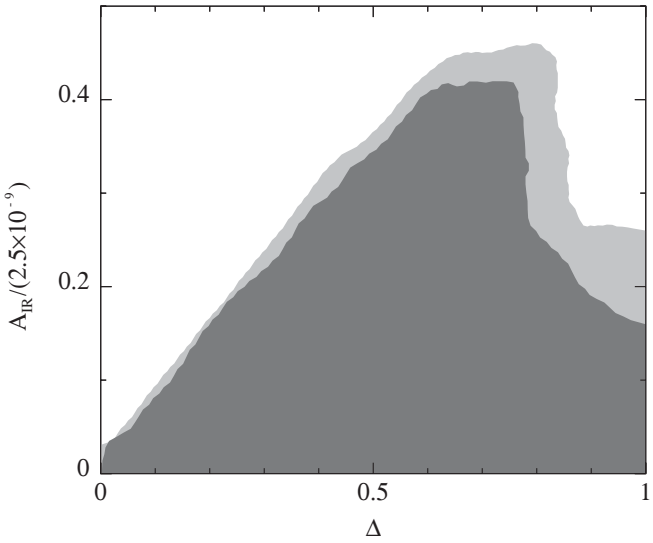

FIG. 5. Marginalized posterior likelihood contours for the parameters A_{IR} and Δ (the feature amplitude and spacing, respectively) of the multiple-bump model. Black and grey regions correspond to values allowed at 95.4% and 99.7% confidence levels, respectively.

TABLE III. Constraints on the standard (vanilla) cosmological parameters for the multiple-bump model. All error bars are at the 95.4% confidence level.

$\Omega_b h^2$	$0.0227^{+0.0009}_{-0.0009}$
$\Omega_c h^2$	$0.1126^{+0.0049}_{-0.0044}$
θ	$1.0424^{+0.0039}_{-0.0043}$
τ	$0.078^{+0.031}_{-0.026}$
n_s	$0.93^{+0.04}_{-0.17}$
$\ln[10^{10}A_s]$	$2.8^{+0.4}_{-0.9}$
A_{SZ}	$1.60^{+0.77}_{-0.76}$
Ω_m	$0.265^{+0.026}_{-0.021}$
σ_8	$0.807^{+0.034}_{-0.030}$
z_{re}	$10.3^{+2.6}_{-2.5}$
H_0	$71.4^{+2.2}_{-2.4}$

fit A_s in Table III is somewhat lower than the standard value and why the spectral tilt $n_s - 1$ is somewhat more red.

To get some intuition for the kinds of multibump distortions that are allowed by the data, we consider an example with $A_{IR} = 1 \times 10^{-9}$, $\Delta = 0.75$ and fix the vanilla parameters to $A_s = 1.04 \times 10^{-9}$, $n_s = 0.93$. This choice of parameters is consistent with the data at 2σ and corresponds to a reasonable coupling $g^2 \sim 0.02$. In Fig. 6 we plot the primordial power spectrum $P(k)$ and also the CMB TT angular power spectrum for this example.

V. PARTICLE PHYSICS MODELS

From the low energy perspective one expects interactions of the type (1) to be rather generic; hence particle production during inflation may be expected in a wide variety of models. In this section we consider some explicit examples in string theory and SUSY in order to show how such models may be obtained microscopically and also to provide the proof of concept that realistic models do exist where ϕ_i are in the observable range.

A. Open string inflation models

String theory inflation models may be divided into two classes depending on the origin of the inflaton: closed string models and open string models. In the former case the inflaton is typically a geometrical modulus associated with the compactification manifold (examples include racetrack inflation [83], Kähler modulus inflation [84], and Roulette inflation [85]). In the latter case the inflaton is typically the position modulus of some mobile D-brane[5] living in the compactification manifold (examples include brane inflation [87] such as the warped KKLMMT model [88], D3/D7 inflation [89], and Dirac-Born-Infeld inflation [90]). In open string inflation models there may be, in addition to the mobile inflationary brane, some additional ''spectator'' branes. If the mobile brane collides with any spectator brane during inflation, then some of the stretched string states between these branes will become massless at the moment when the branes are coincident [14,15], precisely mimicking the interaction (1). Thus, we expect particle production, IR cascading, and the bumplike features described above to be a reasonably generic prediction of open string inflation.

B. String monodromy models

A concrete example of the heuristic scenario discussed in the last subsection is provided by the brane monodromy and axion monodromy string theory inflation models proposed in [18–20]. In the original brane monodromy model [18] one considers type IIA string theory compactified on a nil manifold that is the product of two twisted tori. The metric on each of these twisted tori has the form

$$\frac{ds^2}{\alpha'} = L_{u_1}^2 du_1^2 + L_{u_2}^2 du_2^2 + L_x^2 (dx' + M u_1 du_2)^2, \quad (6)$$

where $x' = x - \frac{M}{2} u_1 u_2$ and M is an integer flux number. The dimensionless constants L_{u_1}, L_{u_2}, and L_x determine the size of the compactification.

Inflation is realized by the motion of a D4-brane along the direction u_1 of the internal manifold. The D4 spans our large three dimensions and wraps a one-cycle along the direction u_2 of the internal space. The size of this one-cycle, in string units, is given by

$$L = \sqrt{L_{u_2}^2 + L_x^2 M^2 u_1^2}. \quad (7)$$

Hence, the brane prefers to minimize its world volume by

[5]One notable exception is inflation driven by the open string tachyon, for example, nonlocal string field theory models [86].

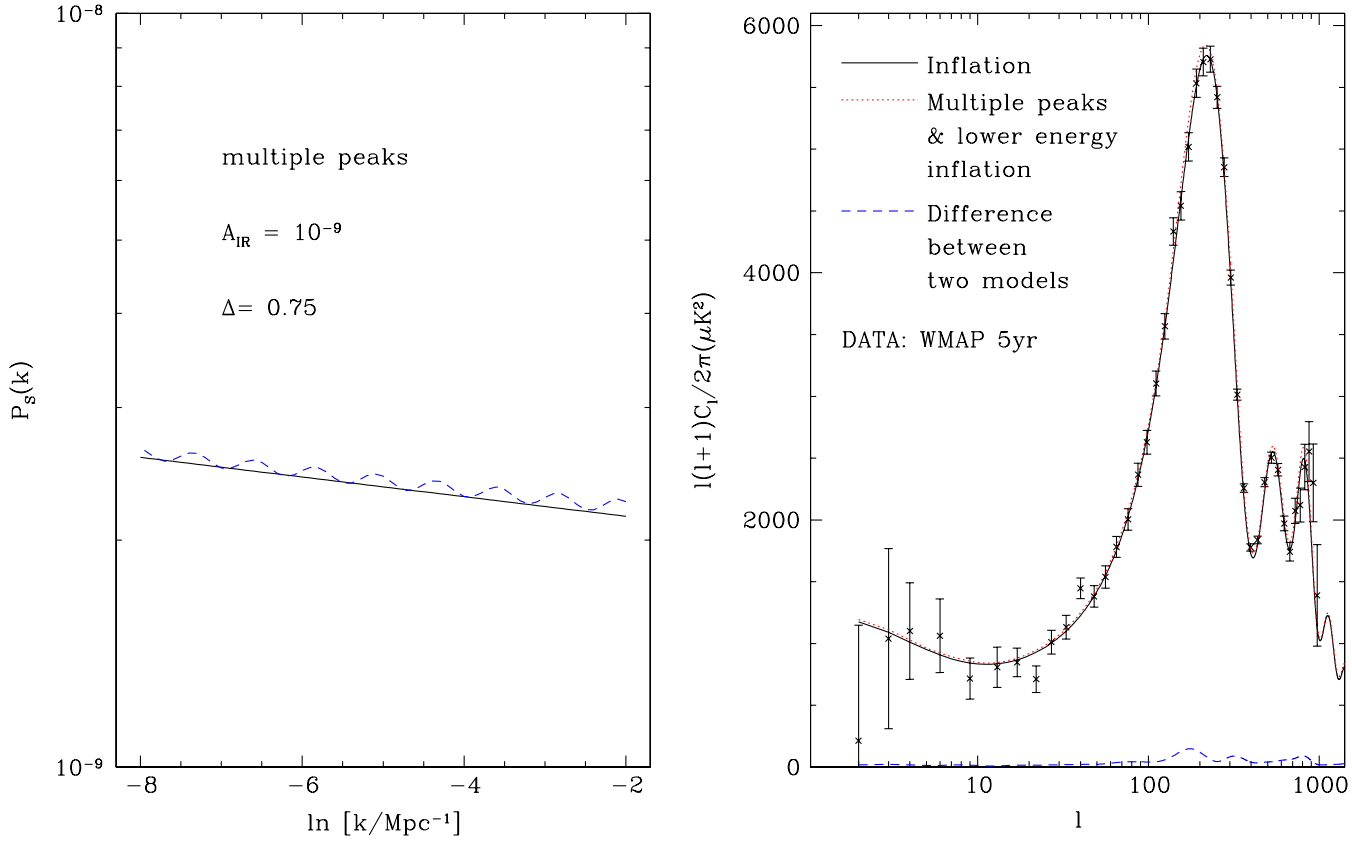

FIG. 6 (color online). The top panel shows a sample multiple-bump distortion with amplitude $A_{\rm IR} = 1 \times 10^{-9}$ which corresponds to $g^2 \sim 0.02$. The feature spacing is $\Delta = 0.75$. We take the vanilla parameters to be $A_s = 1.04 \times 10^{-9}$, $n_s = 0.93$ so that the scale of inflation is slightly lower than in the standard scenario and the spectral tilt is slightly redder. The bottom panel shows the CMB angular TT power spectrum for this example.

moving to the location $u_1 = 0$ where this one-cycle has minimal size. This preference gives a potential to the D4-brane position which goes like $V \sim u_1$ in the large u_1 regime that is relevant for large-field inflation.

In [15] it was shown that this scenario allows for the inclusion of a number of spectator branes stabilized at positions $u_1 = i/M$ (with i integer) along the inflationary trajectory. As the mobile inflationary D4 rolls through these points, particles (strings) will be produced and the resulting distribution of features will look nearly identical to the simple multibump scenario studied in Sec. IV B. To see this, let us now determine the distribution of features that is predicted from brane monodromy inflation. The canonical inflaton ϕ can be related to the position of the mobile D4 as

$$\phi = B u_1^{1/p}, \tag{8}$$

where B is a constant with dimensions of mass that depends on model parameters. Hence, the effective potential during inflation has the power-law form

$$V(\phi) = \mu^{4-p} \phi^p. \tag{9}$$

For the simplest scenario described above one has $p = 2/3$. However, the formulas (8) and (9) still hold for the variant considered in [18] with $p = 2/5$ as long as one replaces u_1 by a more complicated linear combination of coordinates. These relations also hold for axion monodromy models [19] with $p = 1$ and u_1 replaced by the axion, c, arising from a two-form Ramond-Ramond potential $C^{(2)}$ integrated over a two-cycle Σ_2. For *all* models of the form (9) the number of e-foldings N from $\phi = \phi(N)$ to the end of inflation [which occurs at $\phi = p/\sqrt{2}$ when the slow-roll parameter $\epsilon(\phi) = 1$] is given by

$$N = \frac{1}{2p} \frac{\phi^2(N)}{M_p^2} - \frac{p}{4} = \frac{1}{2p} \frac{B^2}{M_p^2} u_1^{2/p} - \frac{p}{4}. \tag{10}$$

Since the spectator branes are located at $u_1 = i/M$ the bursts of particle production must occur at times $N = N_i$, where

$$N_i = \frac{1}{2p} \frac{B^2}{M_p^2} \left(\frac{i}{M}\right)^{2/p} - \frac{p}{4}. \tag{11}$$

The location $k = k_i$ of the ith feature is defined, roughly, by the scale leaving the horizon at the moment $N = N_i$. Hence, the distribution of features for brane/axion monod-

romy models is given by

$$\ln\left[\frac{k_i}{H}\right] \cong \tilde{B}^2 i^{2/p} - \frac{p}{4} \tag{12}$$

with $p = 2/3$ or $p = 2/5$ for brane monodromy and $p = 1$ for axion monodromy. In (12) the dimensionless number $\tilde{B}$ depends on model parameters.

Although the distribution of features (12) is not exactly the same as the evenly spaced distribution considered in Sec. IV B, the two are essentially indistinguishable over the range of scales which are probed observationally (corresponding to roughly 10 e-foldings of inflation). The reason for this is simple: The inflaton is nearly constant during the first 10 e-foldings of inflation and hence $\delta N \sim \delta\phi \sim \delta u_1$ within the observable region. It follows that $k_i \cong e^{(i-1)\Delta} k_1$ to a very good approximation for a huge class of models. To see this more concretely in the case at hand, let us compute dN/du_1 from (10). It is straightforward to show that

$$\frac{dN}{du_1} = \frac{1}{p^p} \frac{1}{[2\epsilon(\phi)]^{1-p/2}} \left(\frac{B}{M_p}\right)^p, \tag{13}$$

where

$$\epsilon(\phi) \equiv \frac{M_p^2}{2}\left(\frac{V'}{V}\right)^2 = \frac{p^2}{2}\left(\frac{M_p}{\phi}\right)^2 \tag{14}$$

is the usual slow-roll parameter. Observational constraints on the running of the spectral index imply that $\epsilon(\phi)$ cannot change much over the observable 10 e-foldings of inflation. Since $dN/du_1 \cong$ const to very high accuracy, it follows trivially that $N = N(u_1)$ is very close to linear and $k_i \cong e^{(i-1)\Delta} k_1$ as desired.

In the context of axion monodromy inflation models [19] the multiple-bump features discussed here will be complementary to the oscillatory features described in [20] which result from the sinusoidal modulation of the inflaton potential by instanton effects. If the bursts of particle production are sufficiently densely spaced, then the signal from IR cascading may appear oscillatory; however, it differs from the effect discussed in [20] in both physical origin and functional form.

Let us now estimate the effective value of the couplings g_i^2 appearing in the prototype interaction (3) that are predicted from the simplest brane monodromy model. A complete calculation would involve dimensionally reducing the Dirac-Born-Infeld action describing the brane motion and would require knowledge of the full 10-dimensional geometry with the various embedded branes. For our purposes, however, a simple heuristic estimate for the collision of two D4-branes will suffice. When N D-branes become coincident, the symmetry is enhanced from $U(1)^N$ to a $U(N)$ Yang-Mills gauge theory. The gauge coupling for this Yang-Mills theory is given by

$$g_{\rm YM}^2 = \frac{g_s(2\pi)^2}{L}, \tag{15}$$

where L is the volume of the one-cycle that the D4-branes wrap and is given by (7). If the inflationary brane is at position u_1 and the ith spectator brane is at $u_{1,i}$, then the distance between the two branes is given by

$$d^2 = \alpha' L_{u_1}^2 (u_1 - u_{1,i})^2. \tag{16}$$

The mass of the gauge bosons corresponding to the enhanced symmetry is

$$M_i^2 = g_{\rm YM}^2 \frac{d^2}{(2\pi)^2(\alpha')^2} = \frac{g_s L_{u_1}^2 (u_1 - u_{1,i})^2}{\alpha' \sqrt{L_{u_2}^2 + L_x^2 M^2 u_1^2}}. \tag{17}$$

To put this in the prototype form $M_i^2 = g_i^2(\phi - \phi_i)^2$, we must first convert to the canonical variable ϕ using formula (8) with $p = 2/3$ and

$$B = \frac{M^{1/2}}{6\pi^2} \frac{L_{u_1} L_x^{1/2}}{\sqrt{g_s \alpha'}}. \tag{18}$$

Next, we must Taylor expand the resulting equation about the minimum $\phi = \phi_i$. We find

$$M_i^2 \cong g_i^2(\phi - \phi_i)^2 + \cdots, \tag{19}$$

$$g_i^2 = \frac{16 g_s^2 \pi^4}{M L_x u_{1,i}} \frac{1}{\sqrt{L_{u_2}^2 + L_x^2 M^2 u_{1,i}^2}} = \frac{16 g_s^2 \pi^4}{L_x i} \frac{1}{\sqrt{L_{u_2}^2 + L_x^2 i^2}}, \tag{20}$$

where in the second equality of (20) we have used the fact that $u_{1,i} = i/M$ (with i integer) in the simplest models. We see that the effective couplings g_i^2 become larger as the D4 unwinds during inflation. [The apparent divergence for $u_{1,i} = 0$ in formula (20) is an artifact of the fact that relation (8) is not valid at small values of u_1. This will not concern us here since inflation has already terminated at the point where our formulas break down.]

To compute the amplitude of the bumplike feature produced by brane monodromy inflation, we should take into account also combinatorial factors. When two branes become coincident the symmetry is enhanced from $U(1)^2$ to $U(2)$, so there are $2^2 - 2 = 2$ additional massless spin-1 fields appearing at the brane collision. Thus, using Eq. (5), the amplitude of the feature that will be imprinted in the CMB is

$$A_{i,\rm eff} = 2 \times (2^2 - 2) \times [1.01 \times 10^{-6} \cdot g_i^{15/4}], \tag{21}$$

where the extra factor of 2 counts the polarizations of the massless spin-1 fields. This combinatorial enhancement can be much larger if the inflationary brane collides with a *stack* of spectators.

The above discussion is predicated on the assumption that the original brane monodromy setup [18] is supple-

mented by additional spectator branes. This may seem like an unnecessary contrivance; however, in order for this model to reheat successfully it may be *necessary* to include spectator branes. For example, with the reheating mechanism proposed in [91] semirealistic particle phenomenology can be obtained by confining the standard model (SM) to a D6-brane which wraps the compact space. In order to reheat into SM degrees of freedom we orient this brane so that its world volume is parallel to the mobile (inflationary) D4. In this case the end of inflation involves multiple oscillations of the D4 about the minimum of its potential. At each oscillation the D4 collides with the D6, and SM particles are produced by parametric resonance preheating [36,37]. However, due to the periodic structure of the compactification, D4/D6 collisions will necessarily occur also *during* inflation, leading to IR cascading features in the CMB.

The timing of these D4/D6 collisions was computed in [91] for the minimal $p = 2/3$ brane monodromy model, assuming the same choices of parameters used in [18]. For this particular case there is only one collision (and hence one feature) during the first 10 e-foldings of inflation, and the phenomenology is essentially the same as that considered in Sec. IVA. What is the amplitude of this feature? Assuming, again, the parameters employed in [18] and noting that the first collision takes place at $i = 13$ [91], Eq. (20) gives $g_1^2 \cong 0.001$. From (21) we find the effective amplitude of the feature to be $A_{1,\mathrm{eff}}/A_s \cong 0.01$. This value is well within the observational bounds derived in Sec. IVA.

We stress that the conclusions in the previous paragraph apply *only* for the particular choice of model parameters employed in [18]. There exist other consistent parameter choices for which the simplest brane monodromy model predicts a much higher density of features with much larger amplitude.

Note that both brane and axion monodromy models may be used to realize trapped inflation [15]. Here we are restricting ourselves to the large-field regime where the potential $V = \mu^{4-p}\phi^p$ is flat enough to drive inflation without the need for trapping effects. For a given choice of parameters one should verify that this classical potential dominates over the quantum corrections from particle production.

C. A supersymmetric model

Another microscopic realization of multiple bursts of particle production and IR cascading during inflation which does not rely on string theory can be obtained from the so-called "distributed mass" model derived in [21] with warm inflation [17] in mind; however, the theory works equally well for our scenario. This model is based on $\mathcal{N} = 1$ global SUSY and allows for the inclusion of multiple points along the inflationary trajectory where scalar degrees of freedom and also their associated fermion superpartners become massless. The distribution of features in this setup is essentially arbitrary.

VI. CONCLUSIONS

In this paper we have studied the observational constraints on models with particle production during inflation. We have focused on the simple prototype model (1) for each burst of particle production; however, we expect that our qualitative results will apply also to more complicated models (for example, with gauged interactions or fermion isoinflaton fields) and perhaps also to the case of inflationary phase transitions. We find no evidence for the detection of the features associated with particle production and IR cascading; however, it is interesting to note that rather large localized features are still compatible with the data. Our results differ significantly from previous studies because of a more realistic treatment of the cosmological perturbations in models with particle production. The bounds we have derived on g^2 will play a crucial role in assessing the detectability of the non-Gaussianity produced by particle production and IR cascading.

We have also discussed the implications of our results for popular brane/axion monodromy string theory inflation models. Successful reheating in these constructions may require the inclusion of spectator branes which collide with the mobile D4-brane during inflation, and hence we expect CMB features to be a fairly generic prediction. We have shown that brane/axion monodromy models predict a distribution of bumplike features which are evenly spaced in $\ln k$ over the observable range of scales. In the case of axion monodromy this multiple-bump spectral distortion is complementary to the oscillatory features discussed in [20]. We have also estimated the magnitude of these bumplike features in terms of model parameters.

One motivation for the present study was to determine the extent to which microscopically realistic models such as (1) can reproduce the localized "glitches" in the power spectrum that have been detected (albeit with marginal significance) by several previous studies. These anomalies can be classified as follows:

(1) *Localized power excesses*:

In both [2,33] power spectra with localized spikes were studied, and in both cases marginal evidence was found for the detection of such features. In [31] a nonparametric reconstruction of the power spectrum was performed, and the result is marginally consistent with a power law everywhere; however, several localized spikes are evident in the reconstruction.

Localized excesses are naturally obtained in our model (1). Sadly, however, we did not find that our model fits the data significantly better than the simplest slow-roll inflation scenario. This does not necessarily imply a disagreement with [2,33] since we use a different shaped feature and different data sets.

(Indeed, when the authors of [33] repeat their analysis using the WMAP 5-yr data, they do not obtain a detection [92], consistent with our findings.)

(2) *Localized power deficits*:
In [24] the Richardson-Lucy deconvolution algorithm was used to perform a nonparametric reconstruction of the primordial power spectrum which displayed a prominent IR cutoff near the horizon. In [34] a similar analysis was performed, and the reconstructed power spectrum displays a localized dip in power near $k \sim 0.002\ \mathrm{Mpc}^{-1}$.
Localized deficits *can* be produced by our model (3) but only in a rather contrived way. Hence, we have not focused on such features in Sec. IV.

(3) *Damped oscillations*:
In [11,13,25,26] power spectra with superimposed ringing patterns were studied. Such features provide a marginally improved fit over the simplest power-law model.
As we have discussed in the introduction, damped oscillatory ringing features are not predicted by inflationary particle production. Nor is it clear if such features are predicted by models with phase transitions. (Of course damped oscillations *can* be obtained from a toy model with a step in $V(\phi)$. However, it may be difficult to obtain such a potential from realistic microphysics; generically one expects that any sharp features in $V(\phi)$ will be smoothed out by quantum corrections.)

Finally, let us note that features of the type studied here will lead to other observables beyond the distortion of the primordial power spectrum. In particular, bumps in $P(k)$ will lead to features in the tensor spectrum (resulting from the sourcing of gravitational waves by scalar fluctuations at second order in perturbation theory) and also, possibly, black hole production. In [93,94] these effects were estimated assuming a power spectrum which is qualitatively similar to ours. As discussed in [5], inflationary particle production will also lead to potentially large localized non-Gaussian features in the bispectrum (and higher order statistics) of the cosmological fluctuations. These non-Gaussianities will be discussed in detail in an upcoming work [22].

ACKNOWLEDGMENTS

This work was supported in part by NSERC. We are grateful to J. Cline, N. Dalal, H. Firouzjahi, D. Green, L. Hoi, L. Kofman, P. McDonald, and G. D. Moore for helpful comments and discussions.

[1] D. J. H. Chung, E. W. Kolb, A. Riotto, and I. I. Tkachev, Phys. Rev. D **62**, 043508 (2000).
[2] G. J. Mathews, D. J. H. Chung, K. Ichiki, T. Kajino, and M. Orito, Phys. Rev. D **70**, 083505 (2004).
[3] O. Elgaroy, S. Hannestad, and T. Haugboelle, J. Cosmol. Astropart. Phys. 09 (2003) 008.
[4] A. E. Romano and M. Sasaki, Phys. Rev. D **78**, 103522 (2008).
[5] N. Barnaby, Z. Huang, L. Kofman, and D. Pogosyan, Phys. Rev. D **80**, 043501 (2009).
[6] D. Langlois and L. Sorbo, J. Cosmol. Astropart. Phys. 08 (2009) 014.
[7] L. A. Kofman and A. D. Linde, Nucl. Phys. **B282**, 555 (1987).
[8] L. A. Kofman and D. Y. Pogosian, Phys. Lett. B **214**, 508 (1988).
[9] D. S. Salopek, J. R. Bond, and J. M. Bardeen, Phys. Rev. D **40**, 1753 (1989).
[10] N. Barnaby and J. M. Cline, Phys. Rev. D **73**, 106012 (2006); **75**, 086004 (2007).
[11] J. A. Adams, B. Cresswell, and R. Easther, Phys. Rev. D **64**, 123514 (2001).
[12] P. Hunt and S. Sarkar, Phys. Rev. D **70**, 103518 (2004); **76**, 123504 (2007).
[13] M. J. Mortonson, C. Dvorkin, H. V. Peiris, and W. Hu, Phys. Rev. D **79**, 103519 (2009).
[14] L. Kofman, A. Linde, X. Liu, A. Maloney, L. McAllister, and E. Silverstein, J. High Energy Phys. 05 (2004) 030.
[15] D. Green, B. Horn, L. Senatore, and E. Silverstein, Phys. Rev. D **80**, 063533 (2009).
[16] M. M. Anber and L. Sorbo, arXiv:0908.4089.
[17] A. Berera, Phys. Rev. Lett. **75**, 3218 (1995).
[18] E. Silverstein and A. Westphal, Phys. Rev. D **78**, 106003 (2008).
[19] L. McAllister, E. Silverstein, and A. Westphal, arXiv:0808.0706.
[20] R. Flauger, L. McAllister, E. Pajer, A. Westphal, and G. Xu, arXiv:0907.2916.
[21] A. Berera and T. W. Kephart, Phys. Rev. Lett. **83**, 1084 (1999).
[22] N. Barnaby (work in progress).
[23] S. Hannestad, J. Cosmol. Astropart. Phys. 04 (2004) 002.
[24] A. Shafieloo and T. Souradeep, Phys. Rev. D **70**, 043523 (2004).
[25] A. Shafieloo, T. Souradeep, P. Manimaran, P. K. Panigrahi, and R. Rangarajan, Phys. Rev. D **75**, 123502 (2007).
[26] L. Covi, J. Hamann, A. Melchiorri, A. Slosar, and I. Sorbera, Phys. Rev. D **74**, 083509 (2006).
[27] J. Hamann, L. Covi, A. Melchiorri, and A. Slosar, Phys. Rev. D **76**, 023503 (2007).
[28] P. Mukherjee and Y. Wang, Astrophys. J. **599**, 1 (2003).
[29] N. Kogo, M. Matsumiya, M. Sasaki, and J. Yokoyama, Astrophys. J. **607**, 32 (2004).
[30] R. Nagata and J. Yokoyama, Phys. Rev. D **78**, 123002

(2008).
[31] R. Nagata and J. Yokoyama, Phys. Rev. D **79**, 043010 (2009).
[32] J. M. Cline and L. Hoi, J. Cosmol. Astropart. Phys. 06 (2006) 007.
[33] L. Hoi, J. M. Cline, and G. P. Holder, arXiv:0706.3887.
[34] G. Nicholson and C. R. Contaldi, J. Cosmol. Astropart. Phys. 07 (2009) 011.
[35] C. P. Burgess, J. M. Cline, F. Lemieux, and R. Holman, arXiv:astro-ph/0306236.
[36] L. Kofman, A. D. Linde, and A. A. Starobinsky, Phys. Rev. Lett. **73**, 3195 (1994).
[37] L. Kofman, A. D. Linde, and A. A. Starobinsky, Phys. Rev. D **56**, 3258 (1997).
[38] N. Barnaby (work in progress).
[39] G. N. Felder, J. Garcia-Bellido, P. B. Greene, L. Kofman, A. D. Linde, and I. Tkachev, Phys. Rev. Lett. **87**, 011601 (2001); G. N. Felder, L. Kofman, and A. D. Linde, Phys. Rev. D **64**, 123517 (2001).
[40] R. Lerner and J. McDonald, Phys. Rev. D **79**, 023511 (2009).
[41] A. A. Starobinsky, JETP Lett. **55**, 489 (1992).
[42] M. Joy, V. Sahni, and A. A. Starobinsky, Phys. Rev. D **77**, 023514 (2008).
[43] X. Chen, R. Easther, and E. A. Lim, J. Cosmol. Astropart. Phys. 06 (2007) 023.
[44] X. Chen, R. Easther, and E. A. Lim, J. Cosmol. Astropart. Phys. 04 (2008) 010.
[45] G. Hinshaw *et al.* (WMAP Collaboration), Astrophys. J. Suppl. Ser. **180**, 225 (2009).
[46] A. Lewis and S. Bridle, Phys. Rev. D **66**, 103511 (2002).
[47] E. Komatsu *et al.* (WMAP Collaboration), Astrophys. J. Suppl. Ser. **180**, 330 (2009).
[48] W. C. Jones *et al.*, New Astron. Rev. **50**, 945 (2006).
[49] F. Piacentini *et al.*, Astrophys. J. **647**, 833 (2006).
[50] T. E. Montroy *et al.*, Astrophys. J. **647**, 813 (2006).
[51] M. C. Runyan *et al.*, Astrophys. J. Suppl. Ser. **149**, 265 (2003).
[52] J. H. Goldstein *et al.*, Astrophys. J. **599**, 773 (2003).
[53] C. L. Kuo *et al.*, Astrophys. J. **664**, 687 (2007).
[54] C. L. Reichardt *et al.*, Astrophys. J. **694**, 1200 (2009).
[55] T. J. Pearson *et al.*, Astrophys. J. **591**, 556 (2003).
[56] A. C. S. Readhead *et al.*, Astrophys. J. **609**, 498 (2004).
[57] A. C. S. Readhead *et al.*, arXiv:astro-ph/0409569.
[58] J. J. Sievers *et al.*, Astrophys. J. **660**, 976 (2007).
[59] C. Dickinson *et al.*, Mon. Not. R. Astron. Soc. **353**, 732 (2004).
[60] N. W. Halverson *et al.*, Astrophys. J. **568**, 38 (2002).
[61] E. M. Leitch, J. M. Kovac, N. W. Halverson, J. E. Carlstrom, C. Pryke, and M. W. E. Smith, Astrophys. J. **624**, 10 (2005).
[62] S. Hanany *et al.*, Astrophys. J. **545**, L5 (2000).
[63] R. A. Sunyaev and Y. B. Zeldovich, Comments Astrophys. Space Phys. **4**, 173 (1972).
[64] R. A. Sunyaev and Y. B. Zeldovich, Annu. Rev. Astron. Astrophys. **18**, 537 (1980).
[65] J. R. Bond *et al.*, Astrophys. J. **626**, 12 (2005).
[66] M. Kowalski *et al.* (Supernova Cosmology Project Collaboration), Astrophys. J. **686**, 749 (2008).
[67] S. Cole *et al.* (2dFGRS Collaboration), Mon. Not. R. Astron. Soc. **362**, 505 (2005).
[68] M. Tegmark *et al.* (SDSS Collaboration), Phys. Rev. D **74**, 123507 (2006).
[69] R. Massey *et al.*, Astrophys. J. Suppl. Ser. **172**, 239 (2007).
[70] J. Lesgourgues, M. Viel, M. G. Haehnelt, and R. Massey, J. Cosmol. Astropart. Phys. 11 (2007) 008.
[71] H. Hoekstra *et al.*, Astrophys. J. **647**, 116 (2006).
[72] C. Schimd *et al.*, Astron. Astrophys. **463**, 405 (2007).
[73] H. Hoekstra, H. K. C. Yee, M. D. Gladders, L. F. Barrientos, P. B. Hall, and L. Infante, arXiv:astro-ph/0202285.
[74] H. Hoekstra, H. K. C. Yee, and M. D. Gladders, Astrophys. J. **577**, 595 (2002).
[75] L. Van Waerbeke, Y. Mellier, and H. Hoekstra, Astron. Astrophys. **429**, 75 (2005).
[76] J. Benjamin *et al.*, arXiv:astro-ph/0703570.
[77] S. De Lope Amigo, W. Y. Cheung, Z. Huang, and S. P. Ng, J. Cosmol. Astropart. Phys. 06 (2009) 005.
[78] V. Springel *et al.*, Nature (London) **435**, 629 (2005).
[79] N. Dalal, O. Dore, D. Huterer, and A. Shirokov, Phys. Rev. D **77**, 123514 (2008).
[80] M. LoVerde, A. Miller, S. Shandera, and L. Verde, J. Cosmol. Astropart. Phys. 04 (2008) 014.
[81] P. McDonald, Phys. Rev. D **78**, 123519 (2008).
[82] N. Afshordi and A. J. Tolley, Phys. Rev. D **78**, 123507 (2008).
[83] J. J. Blanco-Pillado *et al.*, J. High Energy Phys. 11 (2004) 063.
[84] J. P. Conlon and F. Quevedo, J. High Energy Phys. 01 (2006) 146.
[85] J. R. Bond, L. Kofman, S. Prokushkin, and P. M. Vaudrevange, Phys. Rev. D **75**, 123511 (2007).
[86] N. Barnaby, T. Biswas, and J. M. Cline, J. High Energy Phys. 04 (2007) 056; N. Barnaby and J. M. Cline, J. Cosmol. Astropart. Phys. 07 (2007) 017; 06 (2008) 030; N. Barnaby, D. J. Mulryne, N. J. Nunes, and P. Robinson, J. High Energy Phys. 03 (2009) 018; N. Barnaby, Can. J. Phys. **87**, 189 (2009).
[87] G. R. Dvali and S. H. H. Tye, Phys. Lett. B **450**, 72 (1999); C. P. Burgess, M. Majumdar, D. Nolte, F. Quevedo, G. Rajesh, and R. J. Zhang, J. High Energy Phys. 07 (2001) 047.
[88] S. Kachru, R. Kallosh, A. Linde, J. M. Maldacena, L. P. McAllister, and S. P. Trivedi, J. Cosmol. Astropart. Phys. 10 (2003) 013.
[89] K. Dasgupta, C. Herdeiro, S. Hirano, and R. Kallosh, Phys. Rev. D **65**, 126002 (2002).
[90] M. Alishahiha, E. Silverstein, and D. Tong, Phys. Rev. D **70**, 123505 (2004).
[91] R. H. Brandenberger, A. Knauf, and L. C. Lorenz, J. High Energy Phys. 10 (2008) 110.
[92] J. M. Cline and L. Hoi (private communication).
[93] R. Saito, J. Yokoyama, and R. Nagata, J. Cosmol. Astropart. Phys. 06 (2008) 024.
[94] R. Saito and J. Yokoyama, Phys. Rev. Lett. **102**, 161101 (2009).